Electronic Supplementary Material (ESI) for Journal of Materials Chemistry C.

Electronic Supplementary Information

Conductive single nanowires formed and analysed on microfluidic devices

Yanlong Xing,[a,c] Norbert Esser,[c] Petra S. Dittrich*[, b]

a School of Analytical Sciences Adlershof, Humboldt-Universität zu Berlin, Germany;

b Department of Biosystems Science and Engineering, ETH Zürich, Switzerland;

c Leibniz-Institute for Analytical Sciences, ISAS, Berlin, Germany

**E-mail: petra.dittrich@bsse.ethz.ch*

Table of Content

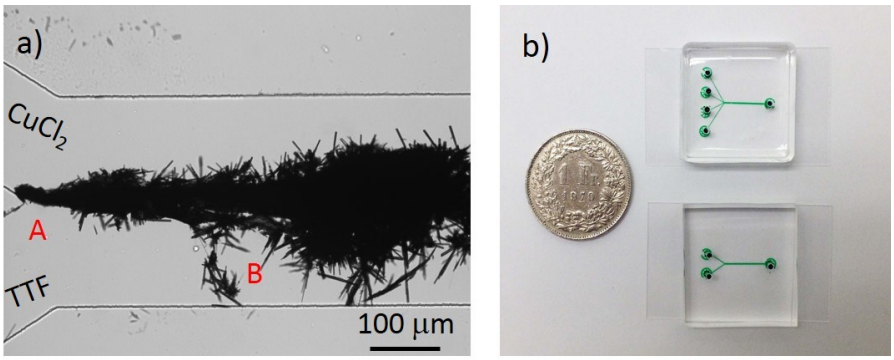

Fig. S1. a) Micrograph of the two-inlet microchip, showing the formation of the reaction product of $CuCl_2$ and TTF (flow rates: 100;100 µL/min). (A) designates the position, where the two precursor solution are in contact first. (B) The reaction product is formed downstream not only at the interface but also nearer the channel walls. b) Photographs of the microchips with a Swiss coin for scale.

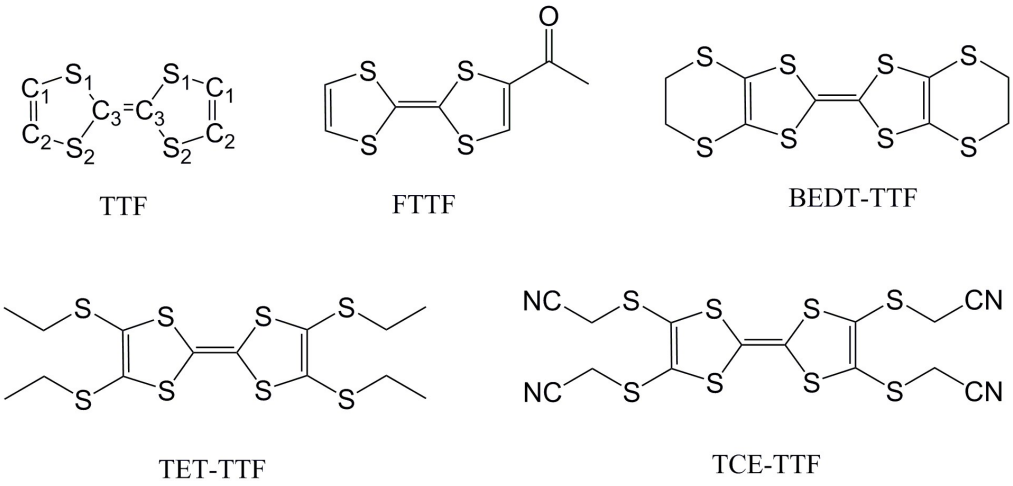

Fig. S2. Chemical structures of TTF derivatives used in this work. TTF: tetrathiafulvalene, FTTF: 2-formyl TTF, BEDT-TTF: bis(ethylenedithio)tetrathiafulvalene, TET-TTF: tetrakis(ethylthio)tetrathiafulvalene and TCE-TTF: 2,3,6,7-Tetrakis(2-cyanoethylthio) tetrathiafulvalene. The labelling of elements of TTF molecule refers to Reference 1.

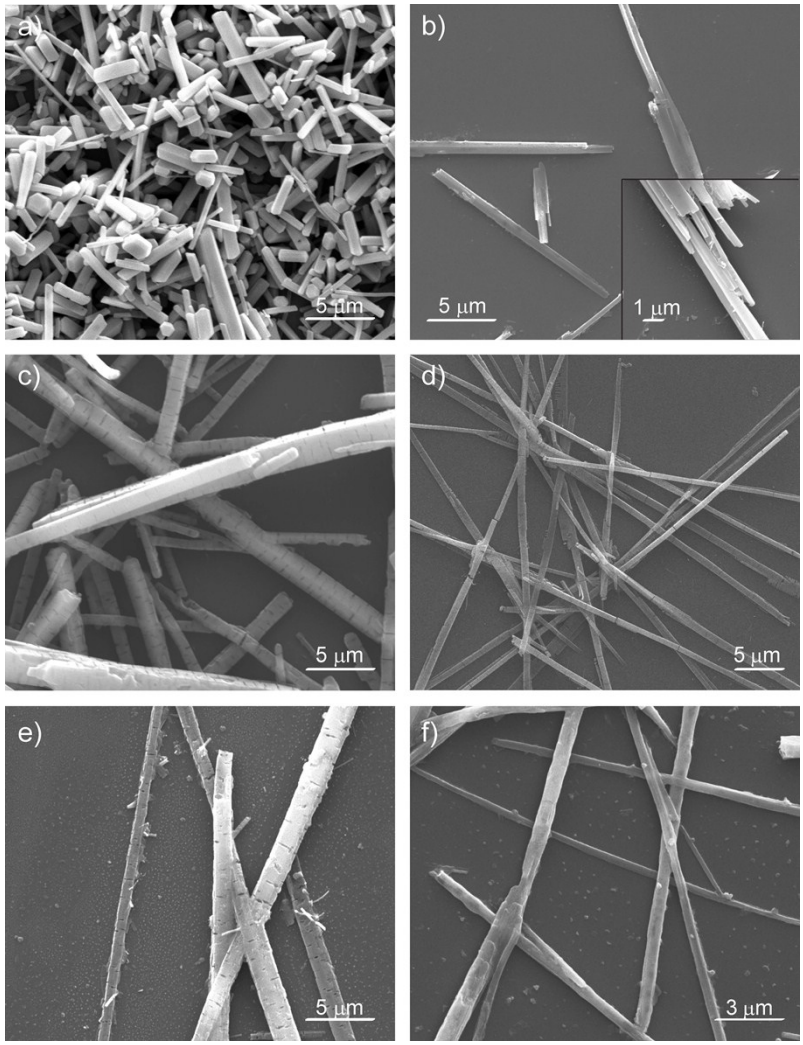

Fig. S3. SEM images of compounds **2b, 3a** and **3b. 2b** generated a) by bulk synthesis and b) on the four-inlet microchip. The inset in b) is a magnified image of the end of a needle structure, showing bundles of wires. c) and d) SEM images of **3a** generated by bulk synthesis and on microchip in CH_3CN. e) and f) SEM images of **3b** generated by bulk synthesis and on the microchip. The numbers of compounds are in accordance with the numbers in Table 1 in manuscript.

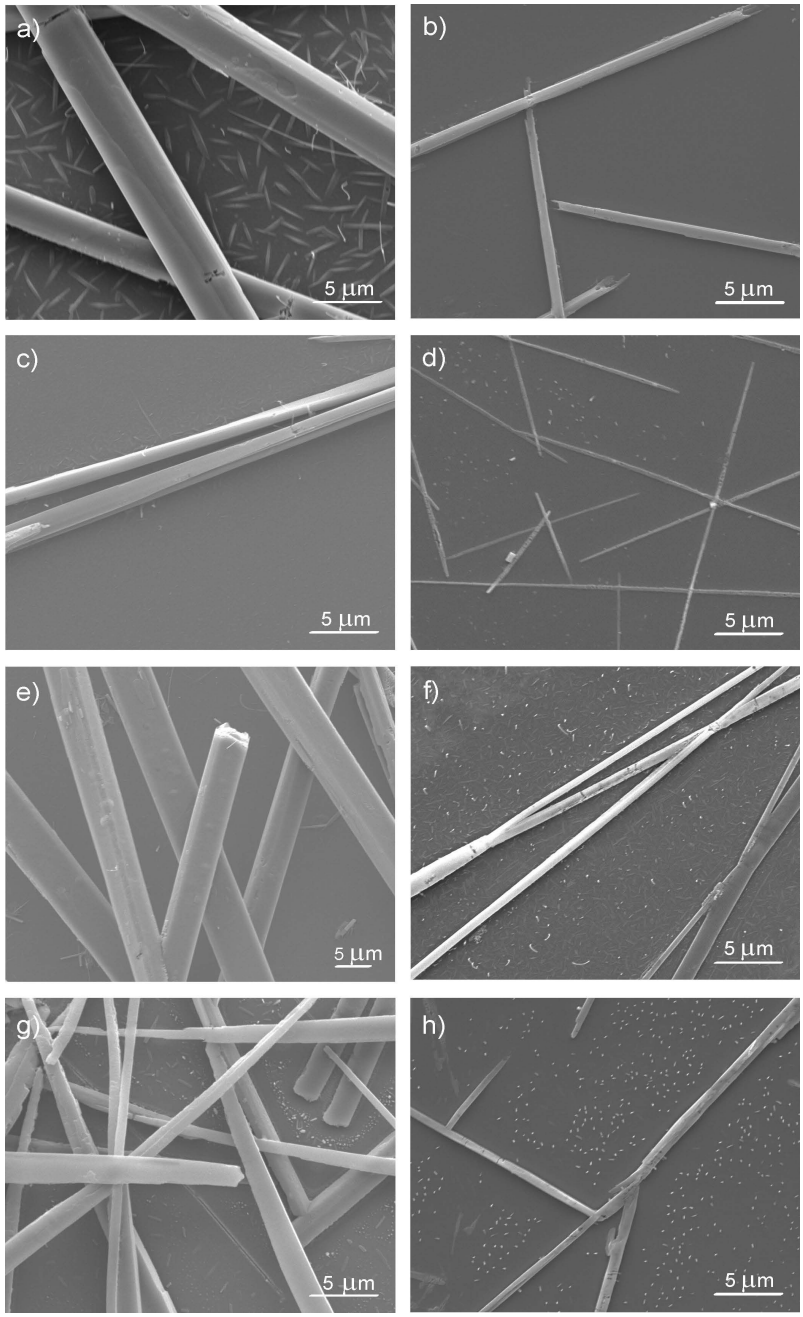

Fig. S4. SEM images of compounds **4a**, **4b, 5a** and **5b.** a) and b) SEM images of **4a** formed in bulk synthesis and on the four-inlet microchip. c) and d) SEM images of **4b** formed in bulk and on microchip. e) and f) SEM images of **5a** generated by bulk synthesis and on microchip. g) and h) SEM images of **5b** generated by bulk synthesis and on microchip. The numbers of compounds are in accordance with the numbers in Table 1 in manuscript.

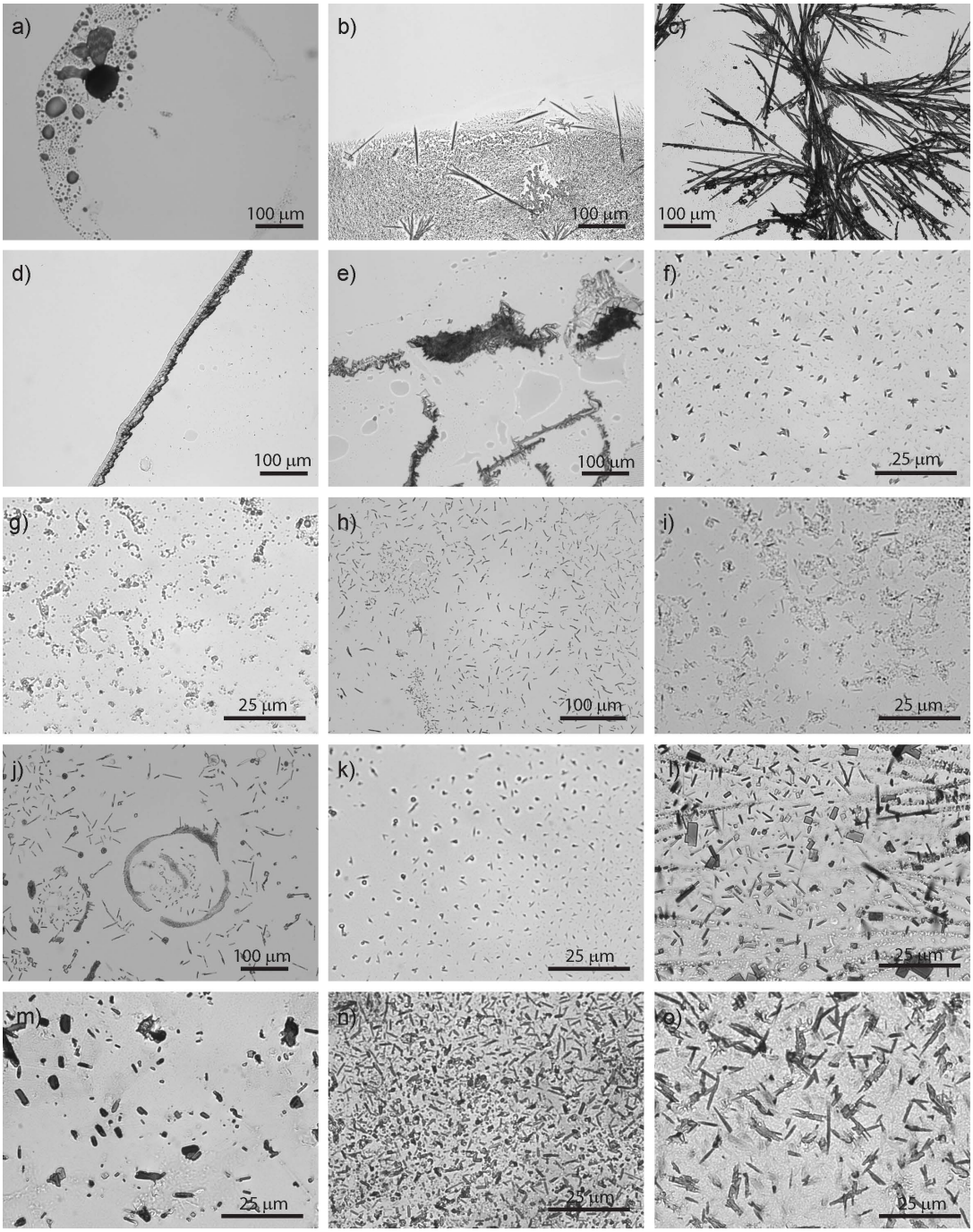

Fig. S5. Optical images of products derived from compounds **6**, **7**, **8**, **9**, **10**, **11**, **12**, **13**, **14**. a) CuCl-TTF (**6**) formed on four-inlet microchip, no obvious structures; $FeCl_2$-TTF (**7**) formed b) in bulk, mixture of needle and small particles, and c) on the two-inlet microchip, large branches of orange crystals; d) $CoCl_2$-TTF (**8**) on four-inlet microchip, no obvious structures; $Co(NO_3)_2$ (**9**) formed e) in bulk, flakes and f) on four-inlet microchip, particles; g) $MnCl_2$-TTF (**10**) on four-inlet microchip, particles; $NiCl_2$-TTF (**11**) formed h) in bulk, mixture of small rods segments and particles, and i) on microchip, particles; $Ni(NO_3)_2$-TTF (**12**) formed j) in bulk, mixture of small rods and particles, and k) on four-inlet microchip, particles; $ZnCl_2$-TTF (**13**) formed l) in bulk, mixture of crystals, rods and particles, and m) on two-inlet microchip, large particles; $Zn(NO_3)_2$-TTF (**14**) formed n) in bulk, cluster of small rods and particles, and o) on two-inlet microchip, needles and crystals. The numbers of compounds are in accordance with the numbers in Table 1 in manuscript.

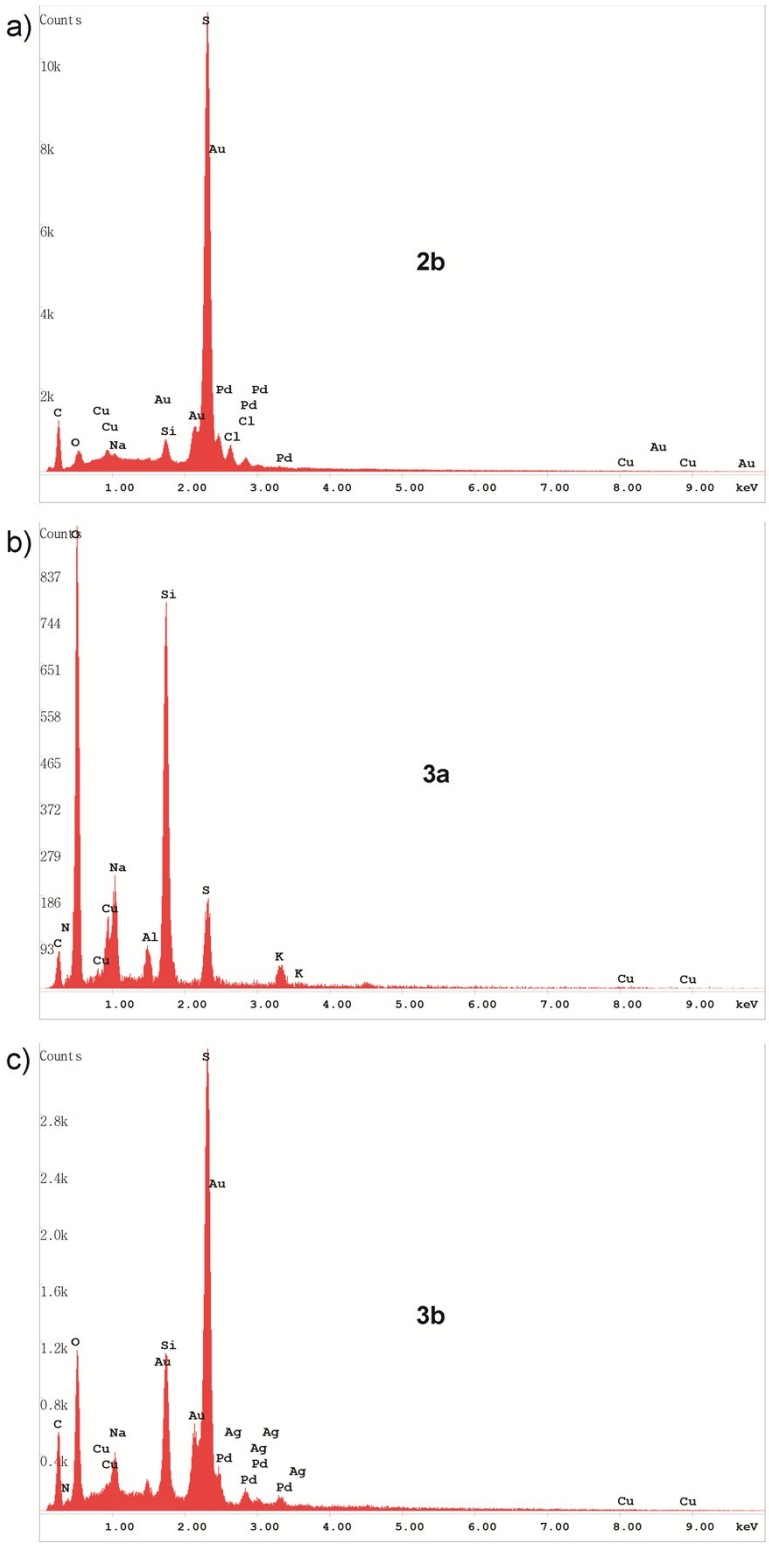

Fig. S6. EDX-SEM spectra of a) $(TTF)_2CuCl_2$ (**2b**), b) $(TTF)_4Cu(NO_3)_2$ (**3a**) and c) $(TTF)_4Cu(NO_3)_2$ (**3b**). Note the presence of Cu and Cl in a) and the presence of N and Cu in c) and d). The small peaks of N was due to its low percentage in the complexes. The numbers of compounds are in accordance with the numbers in Table 1 in manuscript.

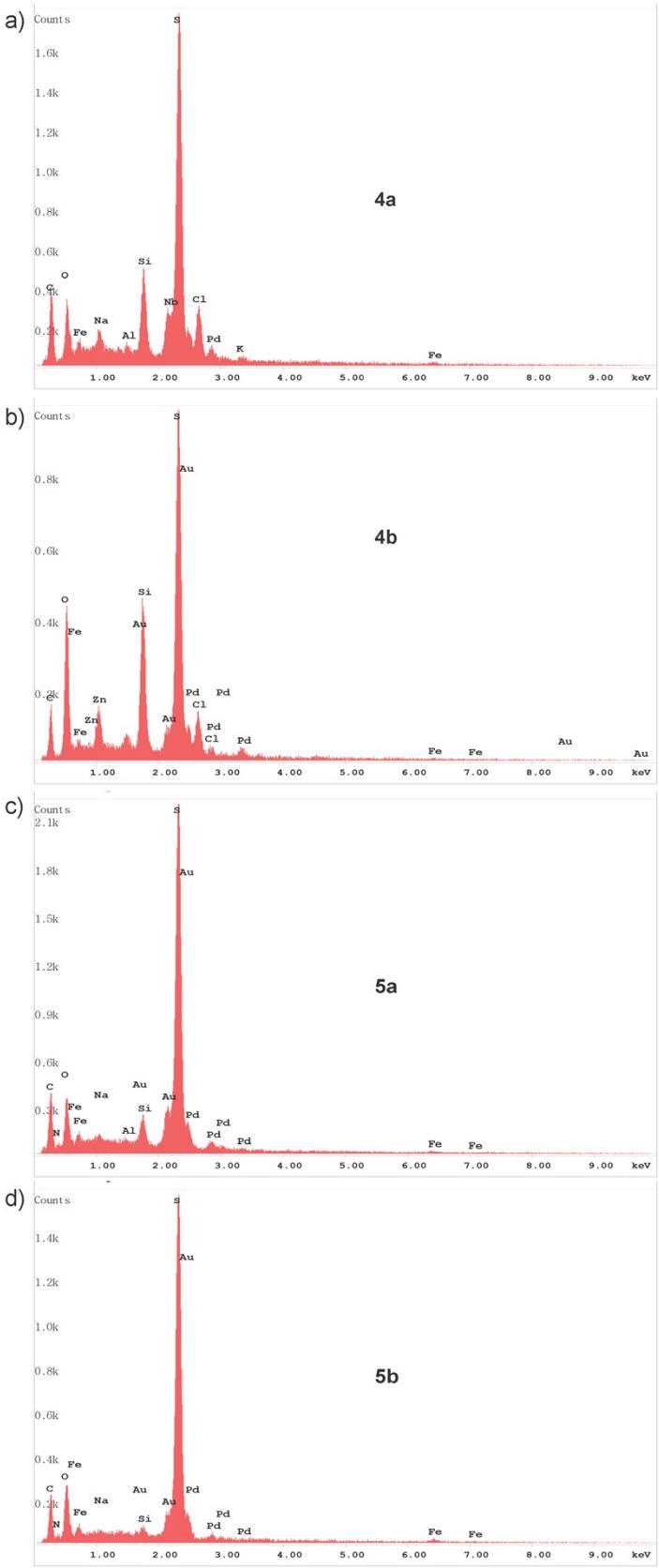

Fig. S7. EDX-SEM spectra of a) $(TTF)_5FeCl_3$ (**4a**), b) $(TTF)_5FeCl_3$ (**4b**), c) $(TTF)_5Fe(NO_3)_3$ (**5a**) and d) $(TTF)_5Fe(NO_3)_3$ (**5b**). Note the presence of Fe and Cl in a) and b), the presence of N and Fe in c) and d). The small peaks of N were due to its low percentage in the complexes. The numbers of compounds are in accordance with the numbers in Table 1 in manuscript.

Table S1. Elemental analysis of compounds **2a, 2b, 3a, 3b, 4a, 4b, 5a** and **5b**

Metal salts	Solvent	Anal. % found (calcd.)			Compound Formula	No.*
		C	H	N		
$CuCl_2$	CH_3CN	28.21 (27.51)	1.53 (1.54)		$(TTF)_7(CuCl_2)_3$	**2a**
$CuCl_2$	CH_3OH	27.20 (26.54)	1.57 (1.48)		$(TTF)_2CuCl_2$	**2b**
$Cu(NO_3)_2$	CH_3CN	28.98 (28.68)	1.77 (1.60)	3.50 (2.79)	$(TTF)_4Cu(NO_3)_2$	**3a**
$Cu(NO_3)_2$	CH_3OH	26.88 (28.68)	1.58 (1.60)	2.88 (2.79)	$(TTF)_4Cu(NO_3)_2$	**3b**
$FeCl_3$	CH_3CN	30.91 (30.43)	2.23 (1.70)		$(TTF)_5FeCl_3$	**4a**
$FeCl_3$	CH_3OH	29.99 (30.43)	2.00 (1.70)		$(TTF)_5FeCl_3$	**4b**
$Fe(NO_3)_3$	CH_3CN	28.77 (28.52)	1.81 (1.60)	3.52 (3.32)	$(TTF)_5Fe(NO_3)_3$	**5a**
$Fe(NO_3)_3$	CH_3OH	28.54 (28.52)	1.81 (1.60)	3.37 (3.32)	$(TTF)_5Fe(NO_3)_3$	**5b**

* The numbers of compounds are in accordance with the numbers in Table 1 in manuscript.

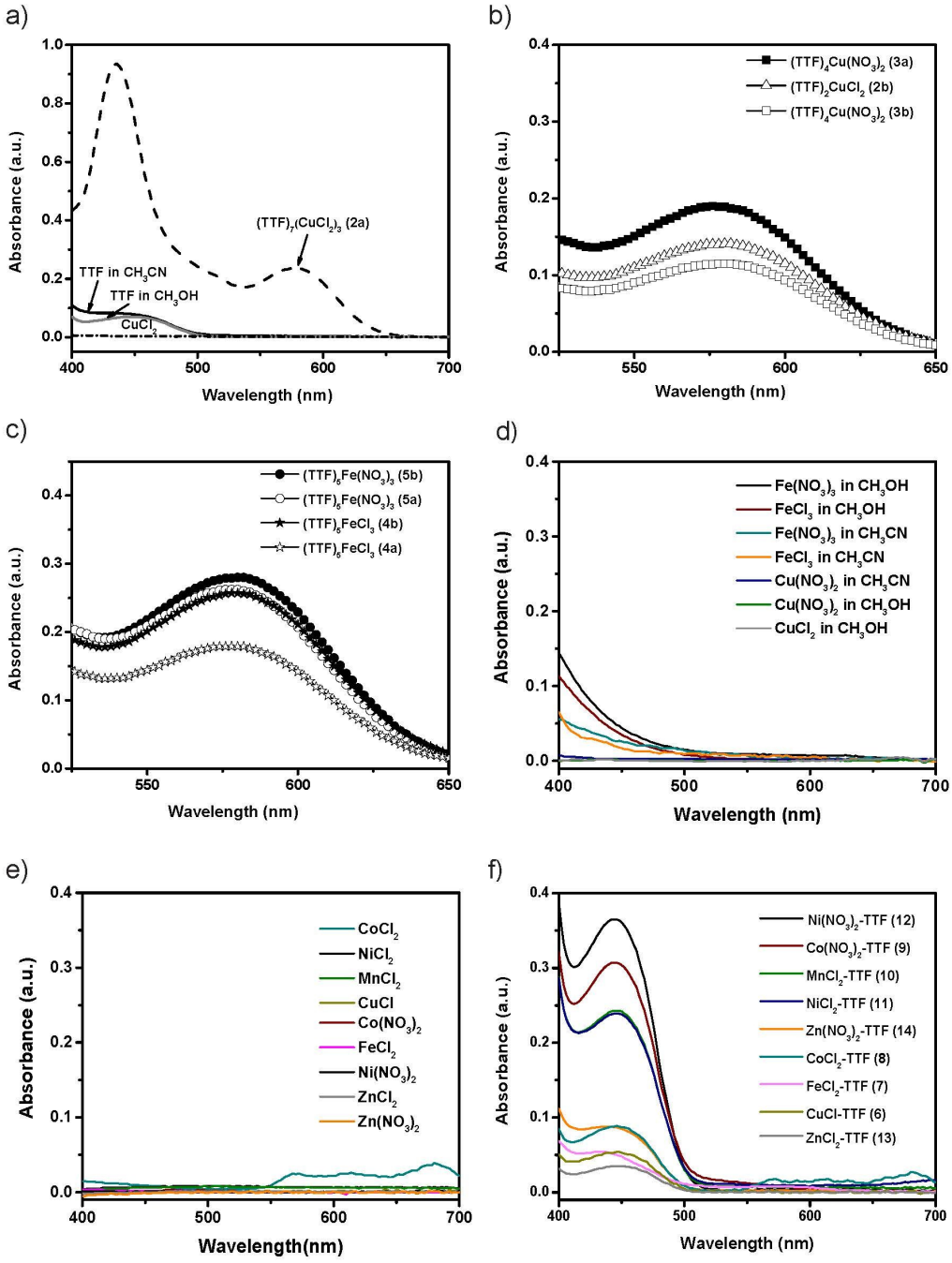

Fig. S8. UV-Vis absorption spectra of solutions of **2a**, **2b**, **3a**, **3b**, **4a**, **4b**, **5a**, **5b**, **6**, **7**, **8**, **9**, **10**, **11**, **12**, **13** and **14**. a) $CuCl_2$ in CH_3CN (0.06 mM), TTF in CH_3CN and CH_3OH (both are 0.24 mM) and the solution after the reaction of $CuCl_2$ and TTF in CH_3CN. A new absorption band at 580 nm (A = 0.237) appeared after formation of the complex **2a**. The absorption band at 580 nm of different charge transfer complexes in different solvents: b) **3a** (A = 0.189), **2b** (A = 0.141) and **3b** (A = 0.115); c) **5b** (A = 0.28), **5a** (A = 0.262), **4b** (A = 0.257) and **4a** (A = 0.179); d) Fe(III) and Cu(II) salts in CH_3CN and CH_3OH; e) Metal salts of Cu(I), Fe(II), Co(II), Mn(II), Ni(II), Zn(II); f) Solution after the reaction of TTF and metal ions in e). **6**, **7**, **8**, **9**, **10**, **11**, **12**, **13**, **14**. The final concentrations of all metal salts were 0.06 mM. The elutes of microreactions were diluted to approx. 0.06 mM. The numbers of compounds are in accordance with the numbers in Table 1 in manuscript.

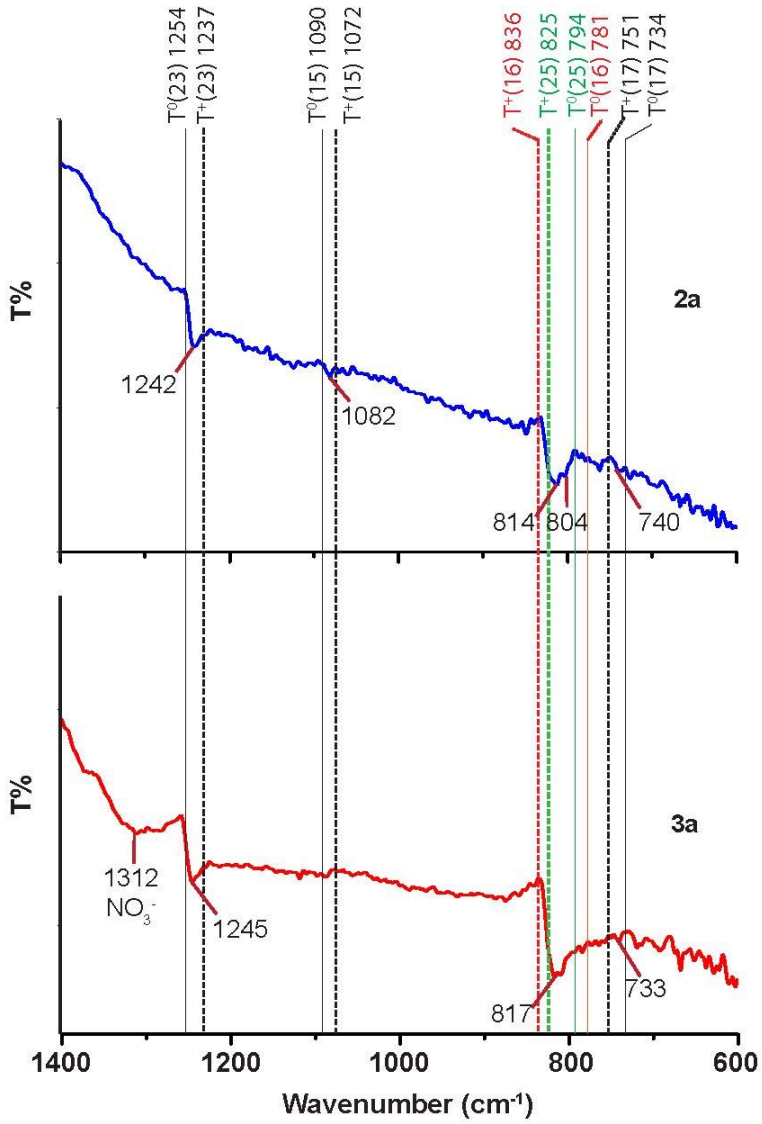

Fig. S9. IR spectra of compounds $(TTF)_7(CuCl_2)_3$ (**2a**)and $(TTF)_4Cu(NO_3)_2$ (**3a**). In the spectrum of **2a**, typical assignments at 1242 cm^{-1} (ν_{23}, CCH bend), 1082 cm^{-1} (ν_{15}, CCH bend), 814 cm^{-1} (ν_{16}, CS stretch), 804 cm^{-1} (ν_{25}, SCC bend), 740 cm^{-1} (ν_{17}, CS stretch) were shown. In the spectrum of **3a**, typical bands were observed at 1245 cm^{-1} (ν_{23}, CCH bend), 817 cm^{-1} (ν_{16}, CS stretch) and 733 cm^{-1} (ν_{17}, CS stretch), the peak at 1312 cm^{-1} indicated the existence of nitrate (NO_3^-). Products were obtained on four-inlet microchips. The wavenumbers of the different vibrational bands are shown at the top for TTF^0 (T^0, solid line) and the cation TTF^+ (T^+, dash line). The numbering of the vibrational modes is given in Ref. 2. The numbers of compounds are in accordance with the numbers in Table 1 in manuscript.

Table S2. IR spectra data of compounds **2b**, **3b**, **4a**, **4b**, **5a** and **5b**

Compound	IR spectra* (cm^{-1})
2b	1245(ν_{23}, CCH bend), 1078 (ν_{15}, CCH bend), 814 (ν_{16}, CS stretch), 803 (ν_{25}, SCC bend)
3b	1319 (NO_3^{-1}), 1247 (ν_{23}, CCH bend), 820 (ν_{16}, CS stretch)
4a	1243 (ν_{23}, CCH bend), 1076 (ν_{15}, CCH bend), 823 (ν_{16}, CS stretch), 800 (ν_{25}, SCC bend), 743 (ν_{17}, CS stretch)
4b	1236 (ν_{23}, CCH bend), 1076 (ν_{15}, CCH bend), 823 (ν_{16}, CS stretch)
5a	1318 (NO_3^{-}), 1243 (ν_{23}, CCH bend), 827 (ν_{16}, CS stretch)
5b	1314 (NO_3^{-}), 1247 (ν_{23}, CCH bend), 818 (ν_{16}, CS stretch)

Note: Compounds were obtained on four-inlet microchips. The numbers of compounds are in accordance with the numbers in Table 1 in manuscript.
*The numbering of the vibrational modes is given in Reference 2. The IR spectra information of nitrate is given in Reference 3.

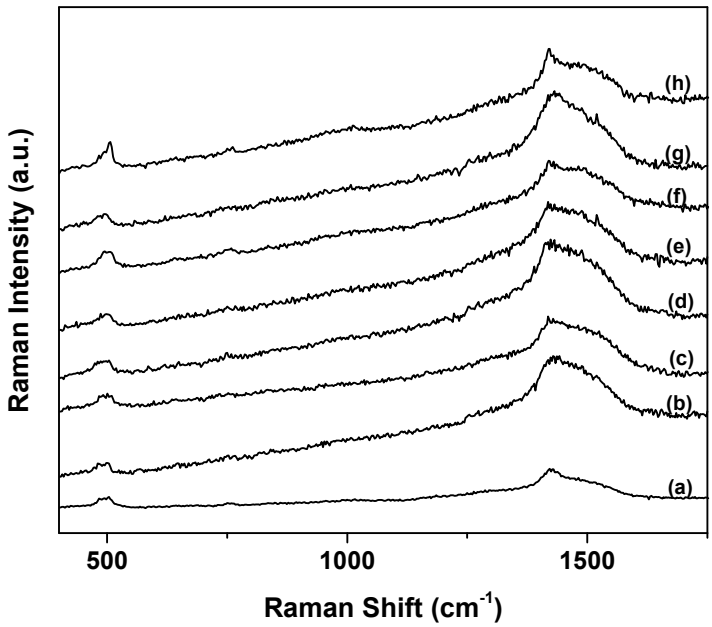

Fig. S10. Raman spectra of compounds **2a**, **2b**, **3b**, **4a**, **4b**, **5a** and **5b** at 532 nm excitation. (a) **2a** (b) **2b**, (c) **3a**, (d) **3b**, (e) **5a**, (f) **5b** (g) **4a**, (h) **4b**. The Raman peaks at around 500 cm^{-1} and 1420 cm^{-1}. The numbers of compounds are in accordance with the numbers in Table 1 in manuscript.

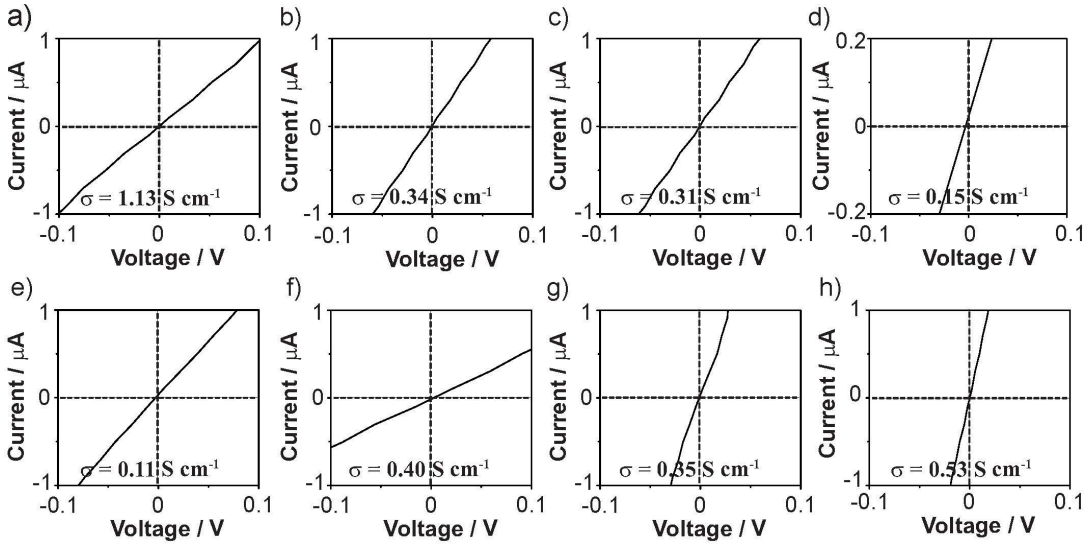

Fig. S11. Linear range of the *I-V* curves in Fig. 2 (in manuscript) and the electrical conductivities of the single nanowires of **2a**, **2b**, **3a**, **3b**, **4a**, **4b**, **5a** and **5b**. a) **2a**, σ = 1.13 S cm^{-1}, b) **2b**, σ = 0.34 S cm^{-1}; c) **3a**, σ = 0.31 S cm^{-1} ; d) **3b**, σ = 0.15 S cm^{-1} (here the *I-V* curve showed linearity between -0.02 μA and 0.02 μA) ; e) **4a**, σ = 0.11 S cm^{-1} ; f) **4b**, σ = 0.40 S cm^{-1}; g) **5a**, σ = 0.35 S cm^{-1}; h) **5b**, σ = 0.53 S cm^{-1}. σ refers to the conductivities at room temperature. The numbers of compounds are in accordance with the numbers in Table 1 in manuscript.

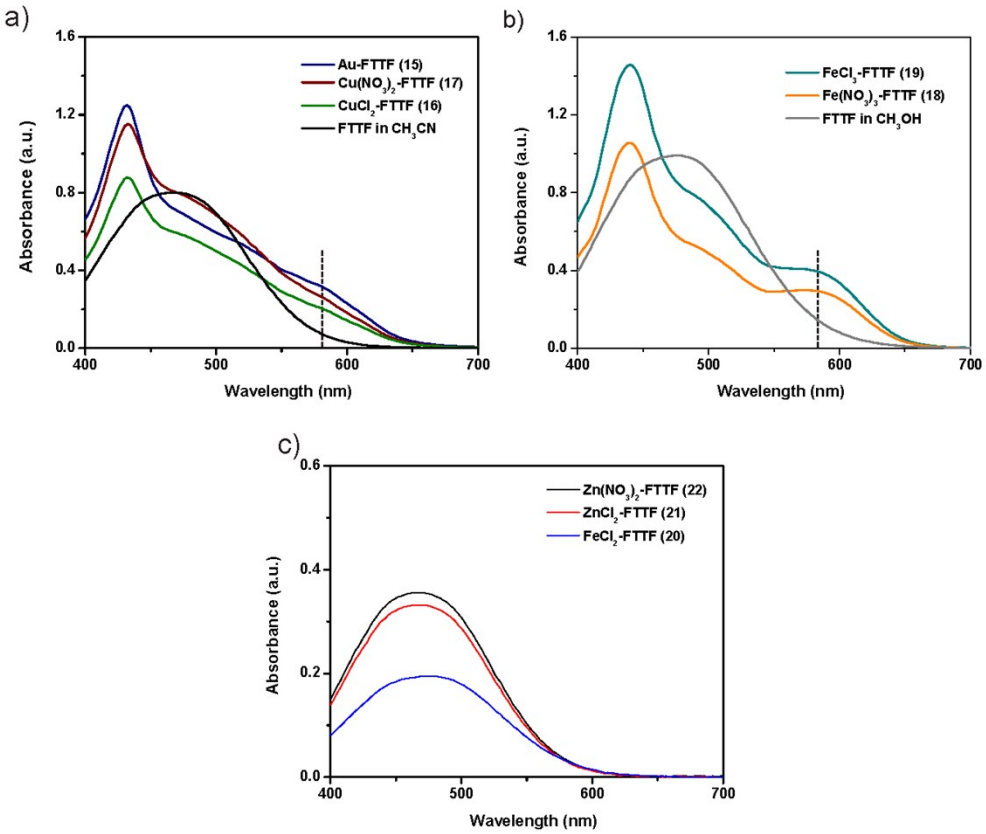

Fig. S12. UV-Vis absorption spectra of the solutions of **15**, **16**, **17**, **18**, **19**, **20**, **21** and **22**. a) **15**, **17**, **16** and pure FTTF in CH_3CN, b) **19**, **18** and pure FTTF in CH_3OH. c) **22**, **21** and **20**. Final concentrations for FTTF are 0.24 mM and for other solutions are approx. 0.06 mM. The dash lines in Figure a) and c) show the position of 580 nm. The numbers of compounds are in accordance with the numbers in Table 1 in manuscript.

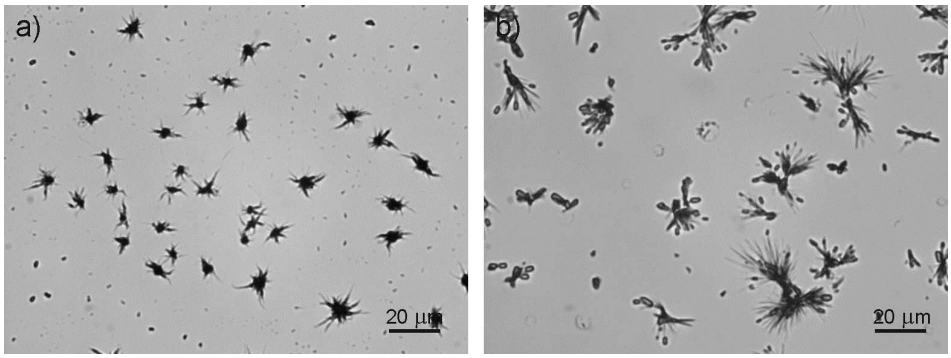

Fig. S13. Optical images of a) Au-FTTF (**15)** and b) Cu-FTTF (**16)** generated by bulk synthesis. Both formed dendritic structures. Scale bars = 20 µm.

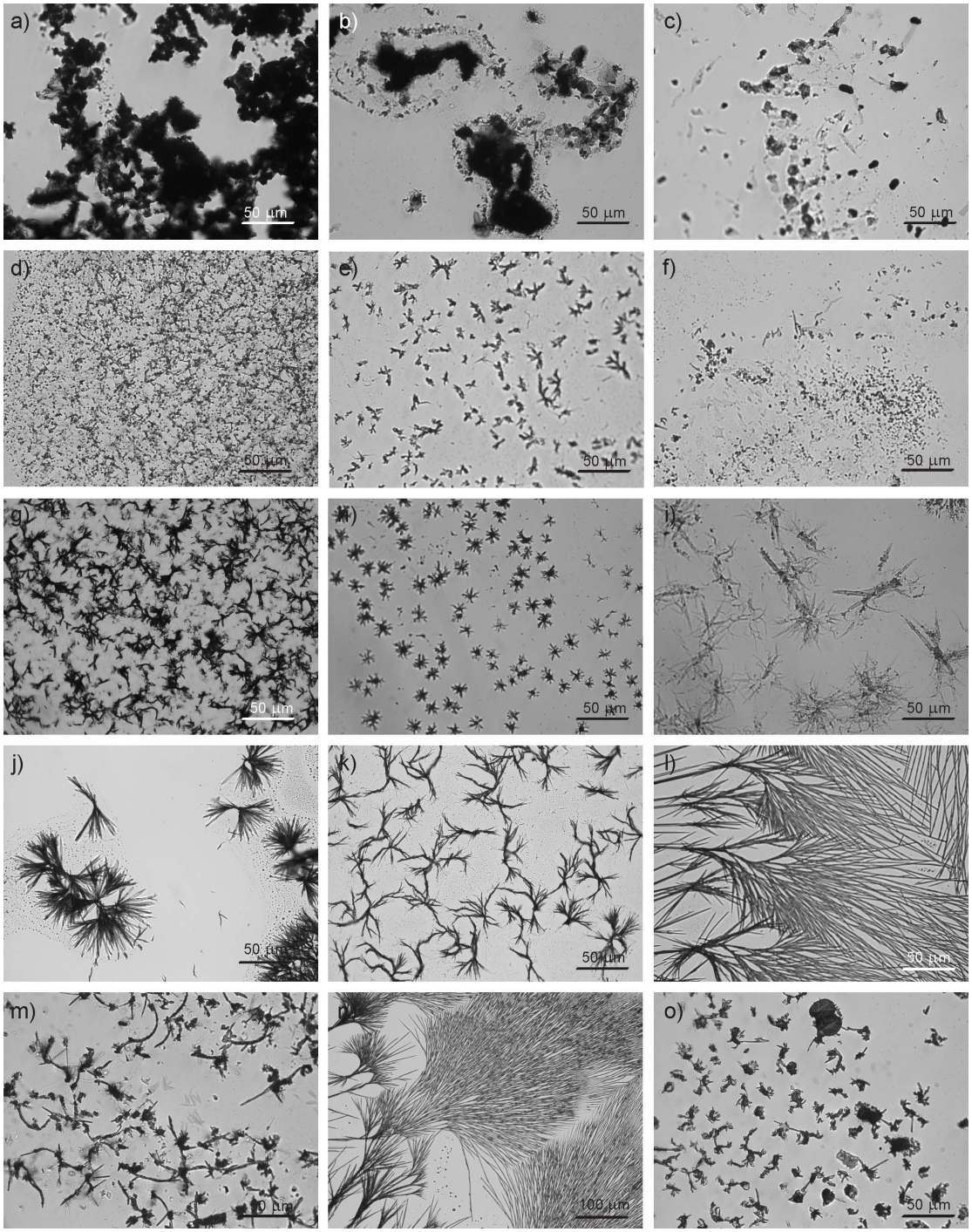

Fig. S14. Optical images of the structures derived from **17**, **18**, **19**, **20**, **21** and **22** in bulk and on microchips: **17** a) in bulk (clusters), b) on the two-inlet chip (clusters) and c) the four-inlet chip (particles). **18** d) in bulk (clusters), e) on the two-inlet chip (small dendrites) and f) the four-inlet chip (particles). **19** g) in bulk (small dendrites), h) on the two-inlet chip (small dendrites) and i) the four-inlet chip (large dendrites). **20** j) in bulk (large dendrites) and k) on the four-inlet chip (small dendrites). **21** l) in bulk (well ordered crystal trees) and m) on the four-inlet chip (large particles). **22** n) in bulk (well ordered crystal trees) and o) on the four-inlet chip (large particles). Note: The structures derived from **20**, **21**, and **22** are crystals of FTTF. The numbers of compounds are in accordance with the numbers in Table 1 in manuscript.

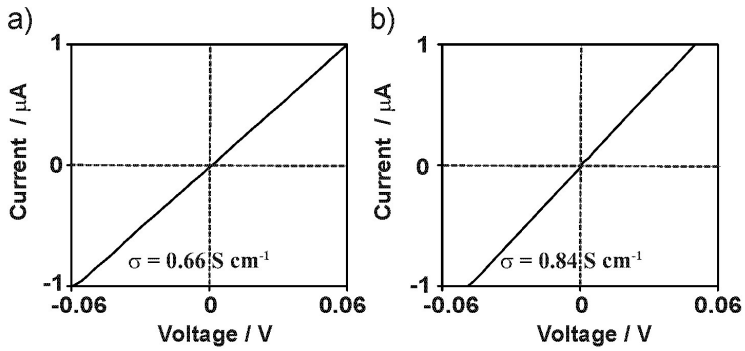

Fig. S15. Linear range of the *I-V* curves in Fig. 3c and 3f (in manuscript) and the electrical conductivities of the single nanowires of **15** and **16**. a) **15**, σ = 0.66 S cm^{-1}, b) **16**, σ = 0.84 S cm^{-1}. σ refers to the conductivity at room temperature. The numbers of compounds are in accordance with the numbers in Table 1 in manuscript.

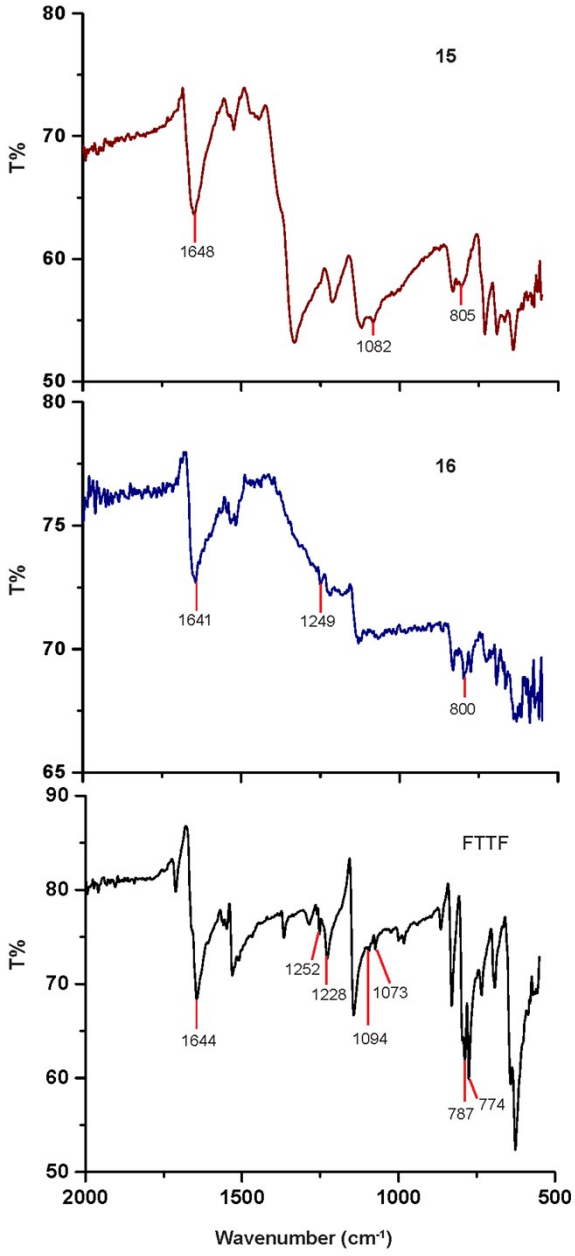

Fig. S16. IR spectra of **15**, **16** and pure FTTF. The numbers of compounds are in accordance with the numbers in Table 1 in manuscript.

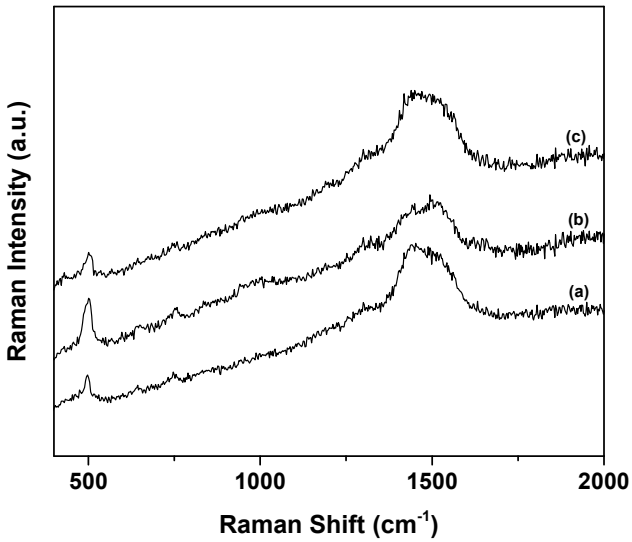

Fig. S17. Raman spectra of compounds a) FTFF solid, b) **15** and c) **16** at 532 nm excitation. Raman peaks are at around 500 cm^{-1} and 1440 cm^{-1}. The numbers of compounds are in accordance with the numbers in Table 1 in manuscript.

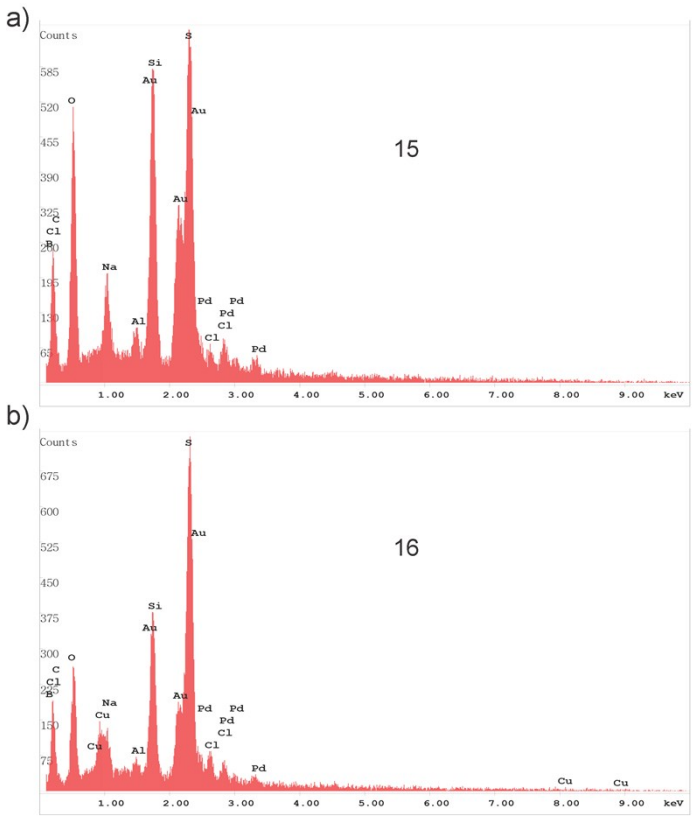

Fig. S18. EDX-SEM spectra of compounds a) **15** and b) **16**. Notice the existence of Cl in figure a), and the existence of Cu and Cl in Figure b). The numbers of compounds are in accordance with the numbers in Table 1 in manuscript.

Table S3. Elemental analysis of **15** and **16** complexes

Metal salts	Solvent	Anal. % found (calcd.)		Compound Formula	No.
		C	H		
$HAuCl_4$	CH_3CN	26.82 (25.21)	1.20 (1.20)	$(FTTF)_3AuCl_3$	**15**
$CuCl_2$	CH_3CN	28.97 (28.07)	1.72 (1.34)	$(FTTF)_2CuCl_2$	**16**

Note: The compound number is in accordance with the numbers in Table 1 in manuscript.

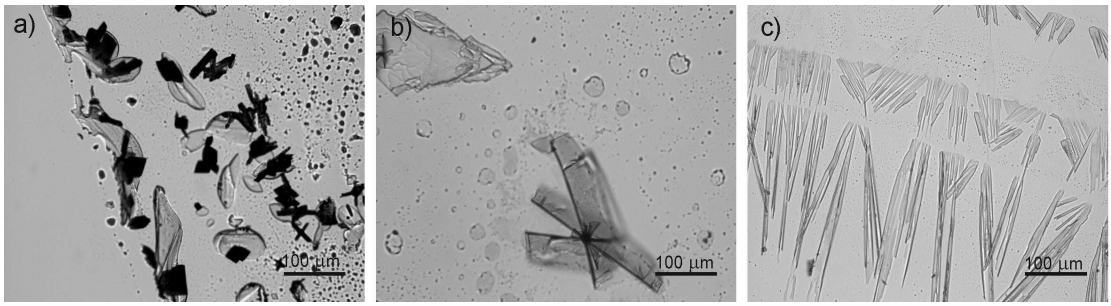

Fig. S19. Optical images of compounds **28**, **29** and **30**. a) **28** (1.5 mM of $HAuCl_4$ and 6 mM of TET-TTF, both in CH_3CN), b) **29** (1.5 mM of $CuCl_2$ and 6 mM of TET-TTF, both in CH_3CN) and c) **30** (0.06 mM of $HAuCl_4$ and 0.24 mM of TCE-TTF, both in CH_3CN) generated on two-inlet microchips seperately. All of them formed flake structures while not wire structures. Scale bars = 100 μm. The numbers of compounds are in accordance with the numbers in Table 1 in manuscript.

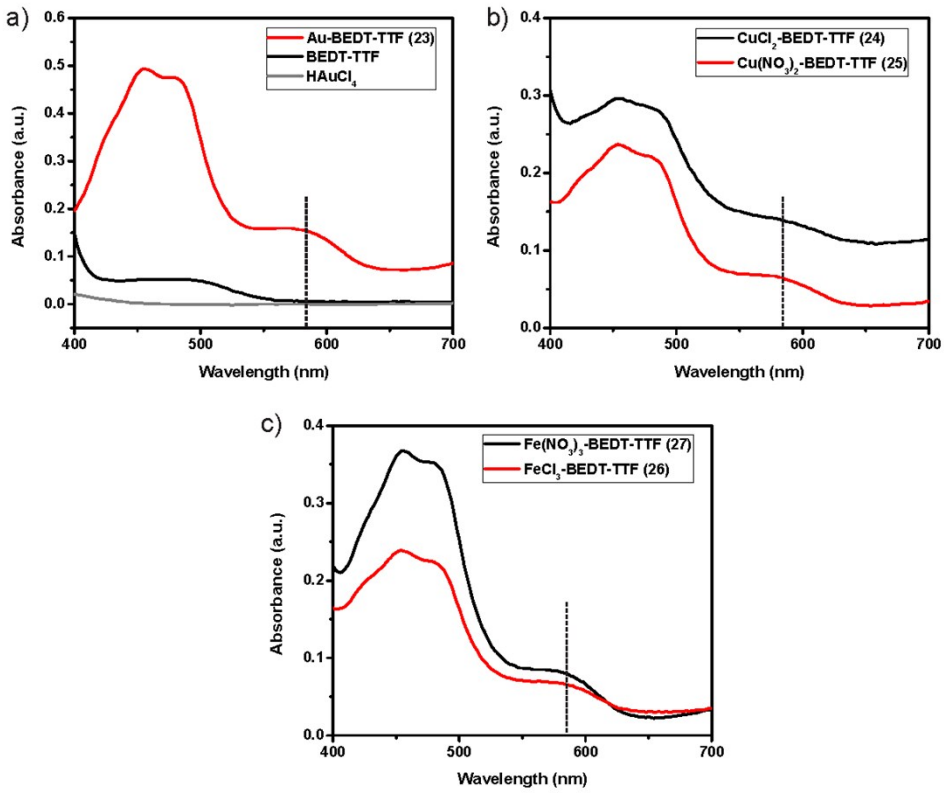

Fig. S20. UV-Vis absorption spectra of the solutions from **23**, **24**, **25**, **26** and **27**. a) **23**, BEDT-TTF in THF, $HAuCl_4$ in CH_3OH, b) **24** and **25**. c) **27** and **26**. Final concentrations for BEDT-TTF are 0.24 mM and for other solutions are approx. 0.06 mM. Note the absorbance at 580 nm for solutions from **23**, **24**, **25**, **26** and **27**. The numbers of compounds are in accordance with the numbers in Table 1 in manuscript.

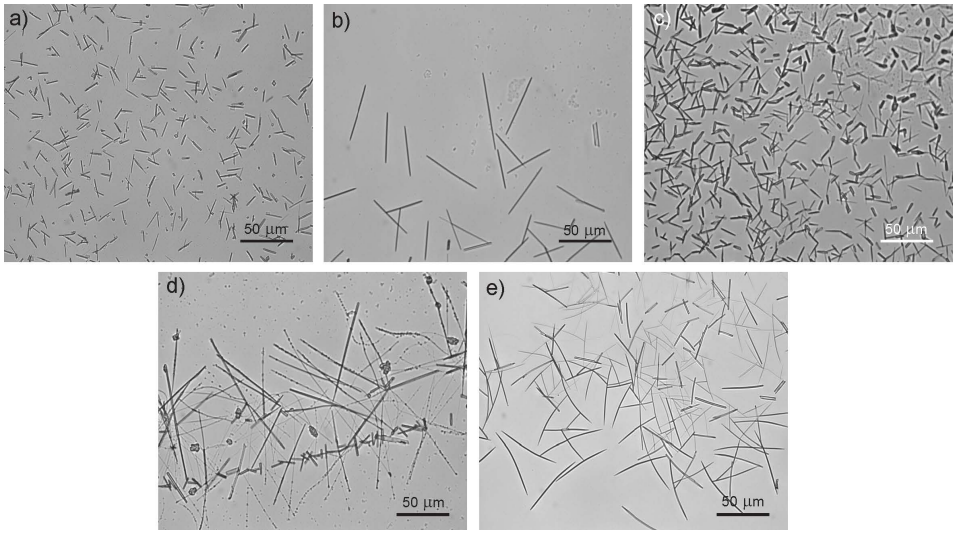

Fig. S21. Optical images of compounds **23**, **24**, **25**, **26** and **27** formed in bulk synthesis. a) **23** (1.73 ± 0.61 µm), b) **24** (1.79 ± 0.31 µm), c) **25** (3.16 ± 0.82 µm), d) **26** (1.68 ± 0.95 µm), and e) **27** (1.29 ± 0.59 µm) formed in bulk synthesis seperately. All of them formed wire like structures. Scale bars = 50 µm. The numbers of compounds are in accordance with the numbers in Table 1 in manuscript.

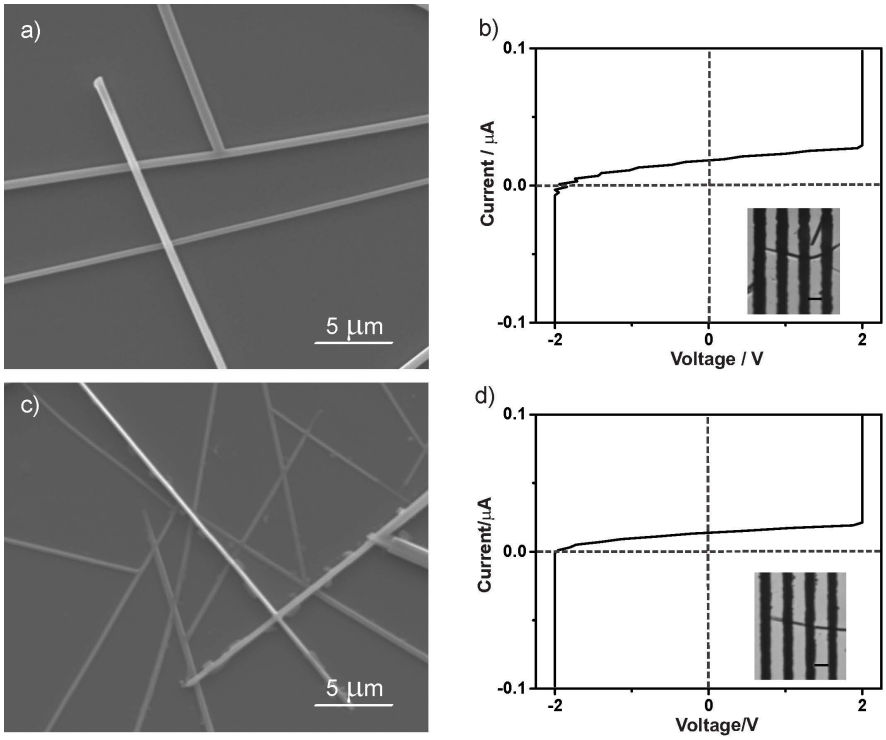

Fig. S22. SEM images and *I-V* curves of structures of **24** and **26**. a) **24** (average diameter, 0.59 ± 0.14 μm). b) *I-V* curve of a single nanowire of **24**. c) SEM images of **26** (average diameter, 0.50 ± 0.12 μm). d) *I-V* curve of a single nanowire of **26**. Figure insets of b) and d) showed the alignment of single nanowires on the microelectrodes. The gaps between the microelectrodes (scale bars) are 5 μm. Note the overload of the curve in Figure b) and d) when we applied the lowest current sweep from -0.1 μA - 0.1 μA using our setup (Keithley 2612 A system source meter). The numbers of compounds are in accordance with the numbers in Table 1 in manuscript.

.

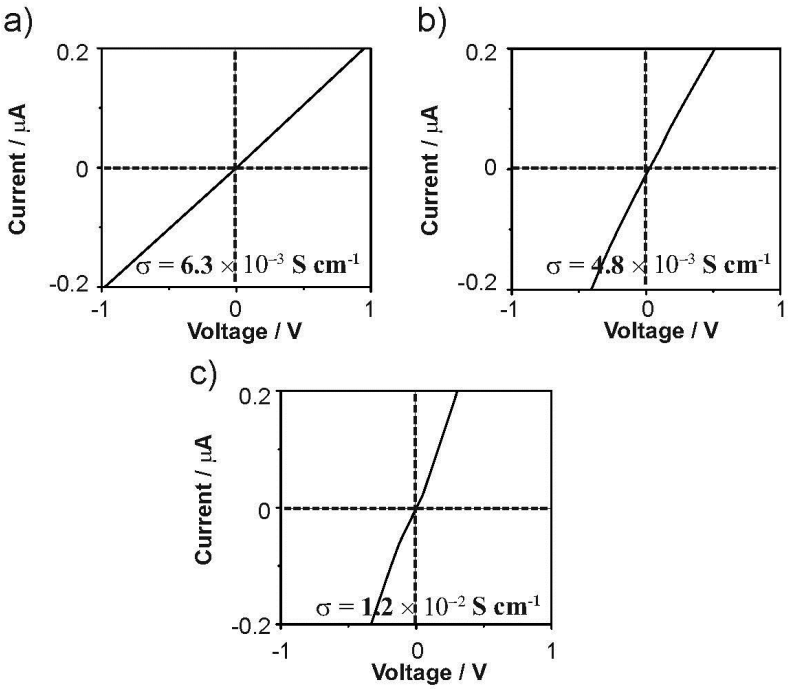

Fig. S23. Linear range of the *I-V* curves in Fig. 4e-4f (in manuscript) and the electrical conductivities of the single nano-/microwires of **23**, **25** and **27**. a) **23,** σ = 6.3 × 10^{-3} S cm^{-1}, b) **25**, σ = 4.8 × 10^{-3} S cm^{-1} and c) **27**, σ = 1.2× 10^{-2} S cm^{-1}. σ refers to the conductivities at room temperature. The numbers of compounds are in accordance with the numbers in Table 1 in manuscript.

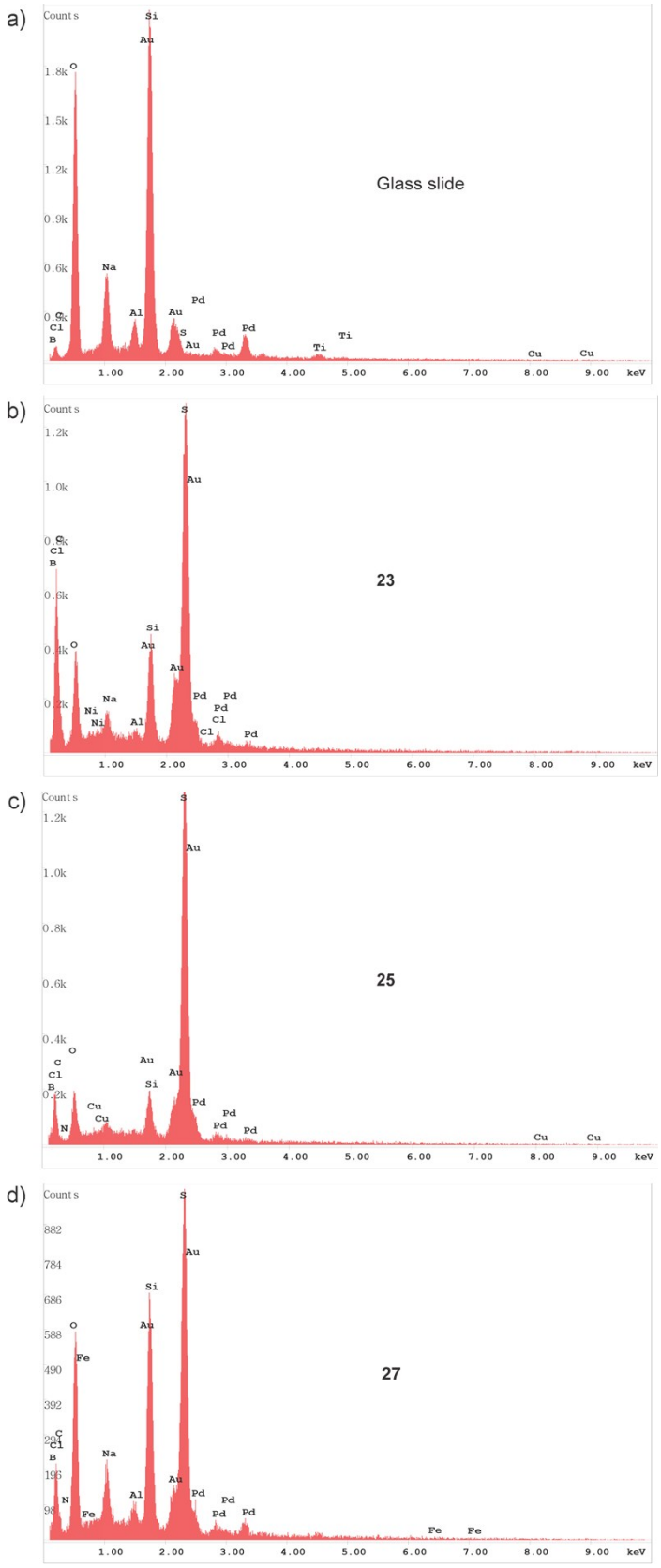

Fig. S24. EDX-SEM spectra of a) Glass slide, b) **23**, c) **25** and d) **27**. Note the increase of C and S in b), c) and d). Also note the existence of Cu and Fe in Figure c) and d). The numbers of compounds are in accordance with the numbers in Table 1 in manuscript.

References:

1. D. J. Sandman, A. J. Epstein, J. S. Chickos, J. Ketchum, J. S. Fu and H. A. Scheraga, *J. Chem. Phys.* 1979, **70**, 305-313.
2. a) R. Bozio, I. Zanon, A. Girlando, C. Pecile, *J. Chem. Phys.* 1979, **71**, 2282-2293; (b) M. B. Inoue, M. Inoue, Q. Fernando, K. W. Nebesny, *Inorg. Chem.* 1986, **25**, 3976-3980; (c) Y. I. Kim, W. E. Hatfield, *Inorg. Chim. Acta*, 1991, **188**, 15-24.
3. N. F. Curtis, Y. M. Curtis, *Inorg. Chem.* 1965, **4**, 804-809.